applied sciences

MDPI

Article

An Overview of Self-Heating Phenomena and Theory Related to Damping and Fatigue of Metals

Xijia Wu * and Lucy Li

Structures and Materials Performance Laboratory, Aerospace Research Center, National Research Council, Ottawa, ON K1A 0R6, Canada; lucy.li@nrc-cnrc.gc.ca
* Correspondence: xijia.wu@nrc-cnrc.gc.ca; Tel.: +1-613-990-5051

Abstract: This paper presents an overview of the self-heating phenomena and the continuum thermodynamics framework related to the damping and fatigue of metals. The self-heating process under cyclic loading generally undergoes three phases: Phase I with gradually increasing temperature to a stabilized or steady-state in Phase II, followed by Phase III with an accelerated temperature increase until the test sample ruptures. Although energy dissipation and heat generation are all captured by the first law of thermodynamics, the functional form of the heat source(s) with entropy change is not formulated for engineering materials. Experimentally, infrared (IR) thermographic techniques can measure the surface temperature variation during constant-amplitude fatigue testing. The observed relationship between the stabilization temperature or temperature increase rate and the applied stress amplitude is often used to infer the fatigue endurance limit, above which point heat generation from "damage" leads to acceleration of self-heating. The IR thermographic fatigue testing offers a rapid alternative method to assess the material's fatigue strength. But, the full physical interpretation of the phenomena remains a challenge. On the other hand, the Tanaka-Mura–Wu model is introduced to describe fatigue crack nucleation via accumulation of dislocation dipole pile-up, which provides a class-A prediction (forecast before even happening) for fatigue crack nucleation life in terms of the material's elastic modulus, Burgers vector, surface energy, and the loading parameter such as cyclic stress/strain range. Then, the release of dislocation dipole pile-up energy to form new crack surfaces is brought into the energy argument. With the inclusion of crack formation energy in the first law of thermodynamics, a unified framework of deformation, damping, fatigue, and self-heating may be established for structural design.

Keywords: fatigue; self-heating; dissipation; damping; thermodynamics

Citation: Wu, X.; Li, L. An Overview of Self-Heating Phenomena and Theory Related to Damping and Fatigue of Metals. *Appl. Sci.* **2022**, *12*, 3054. https://doi.org/10.3390/app12063054

Academic Editors: Ricardo Branco and Mohamed M. Chehimi

Received: 19 January 2022
Accepted: 14 March 2022
Published: 17 March 2022

1. Introduction

Traditionally, for structural design, the fatigue properties of a material need to be determined through a large amount of fatigue testing at many stress levels until down to a stress level with fatigue life exceeding 10^7 cycles. The fatigue data generated this way in stress control are often presented in the form of an S-N curve, first investigated by Wöhler [1]. The stress amplitude at which the material has endured 10^7 fatigue cycles is called the fatigue endurance limit. Such fatigue characterization practices are extremely time-consuming and expensive for industrial design.

In recent years, the phenomena of self-heating in metals and composites during cyclic (or fatigue) loading have attracted a great deal of interest, as it provides an alternative, often rapid method for determination of fatigue endurance limit, as compared to conventional fatigue testing. A method called the Risitano method using infrared thermography techniques was developed to track the temperature increase on the coupon surface with loading cycles (or time), where a transition point in the relationship of sample surface temperature change vs. stress corresponded to the fatigue endurance limit [2]. Following Risitano's work, a significant amount of studies have been carried out on metals [3–30] and

composites as well [31–43]. Physically, the self-heating phenomena are related to energy dissipation and entropy change in damping, thermoelastic, viscoelastic, viscoplastic, and (rate-independent) plastic deformation. Therefore, it is important to understand the different aspects of the self-heating process, to achieve a holistic view of material deformation, energy dissipation, and damage accumulation. Due to the limited space, the current review only focuses on metals, outlined below.

The experimental technique of IR thermographic fatigue is briefly introduced, and the key phenomena of self-heating are summarized in Section 2, representing the points of discussion. The general thermodynamic laws governing heat generation are reviewed in Section 3 with various terms as the heat sources [7,43,44]. In particular, heat sources are classified by their controlling mechanisms, such as thermoelastic deformation (Section 3.1), internal friction (Section 3.2), and intrinsic dissipation (Section 3.3). The laws of thermodynamics govern the heat generation, heat transfer, internal energy, and entropy changes associated with every physical mechanism with the self-heating temperature change as an overall result. Wherever applicable, mathematical equations for the observed calorimetric responses are given, which have been used by researchers to analyze the heat generation mechanisms and responses. Damping is discussed in association with thermographic fatigue in Section 3.4. The concept of fatigue fracture entropy is introduced in Section 3.5 [16]. The dislocation-based Tanaka-Mura-Wu model for fatigue crack nucleation is introduced in Section 3.6 [45,46], which can provide class A prediction of fatigue life, independent of conventional and thermographic fatigue testing. Dislocation dipole pile-ups are formed by alternating slips under cyclic loading, which has been well-recognized as the very mechanism of mechanical fatigue in metallic materials. Thus, the energy release for fatigue crack nucleation is naturally a part of the thermodynamic energy dissipation process. To include the crack formation energy into the thermodynamic framework, energy arguments are discussed in Section 3.7. Critical questions are also raised in discussions to identify the gaps in the current state-of-the-art. It is hoped that a unified thermodynamic framework will be established for deformation, damping, and fatigue, including heat generation, by amending those gaps.

2. Infrared-Thermography Cyclic Test and Self-Heating Phenomena

A typical setup of the infrared (IR)-cyclic thermography test is schematically illustrated in Figure 1. The system employs an infrared camera to record the surface temperature on the fatigue coupon being tested. It sends the signals to a computer, which also receives the temperature measurement signals from a dummy coupon at the ambient temperature but not subjected to loading. All the signals are processed by the computer, where the temperature increments relative to the ambient temperature are calculated and shown on the screen. The fatigue testing is a typical mechanical testing setup (details of load cell and strain measurements are omitted), except that care must be exercised when clamping the specimen at its two ends to minimize heat loss by conduction to the grips.

The typical temperature increment curves are schematically shown in Figure 2. The calorimetric behavior generally consists of three phases. Phase I exhibits a rather steep temperature increase. In phase II, the temperature is often stabilized at a constant level, ΔT_{AS}, or in some cases, it may also increase at nearly a constant rate. Phase III represents an unstable phase of temperature increase up to fracture. The Risitano method determines the fatigue endurance limit by plotting curves of the stabilized temperature increment ΔT_{AS} or the initial rate of temperature increase $\partial T/\partial N$ against the applied stress amplitude σ. The intersection point with a slope change is determined to be the value of the fatigue limit σ_{fl}, as shown in Figure 3. Below this "intersection" point, the self-heating mechanism is effectively "non-damaging", which means that Phase II could last forever; above it, fatigue damage would accumulate and eventually lead to Phase III (fracture). The Risitano method was established on the premise that the temperature increment had a well-defined stabilization stage with a constant ΔT_{AS} at a constant stress amplitude in testing (the gray colored line). Thus, the sudden change in the ΔT_{AS} vs. σ behavior could reflect additional

heat generation mechanisms associated with damage nucleation and propagation; as a result, the point is inferred as the fatigue endurance limit [2]. In the case where the sample surface temperature increases continuously in phase II (the orage colored line) rather than reaching a stabilization temperature, the initial rate of temperature change has been used to correlate with the fatigue life (N_f) [25]. IR-thermography fatigue tests are often carried out at a frequency in the range of 1 to 170 Hz [9,12], depending on the material and specimen configuration, to generate measurable heat.

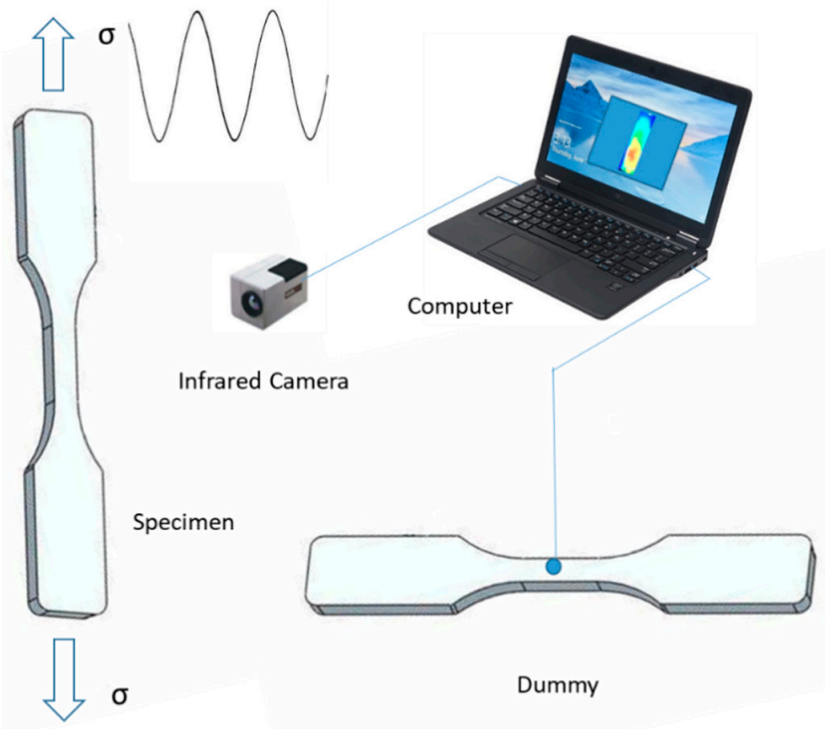

Figure 1. A schematic of the thermographic fatigue test setup.

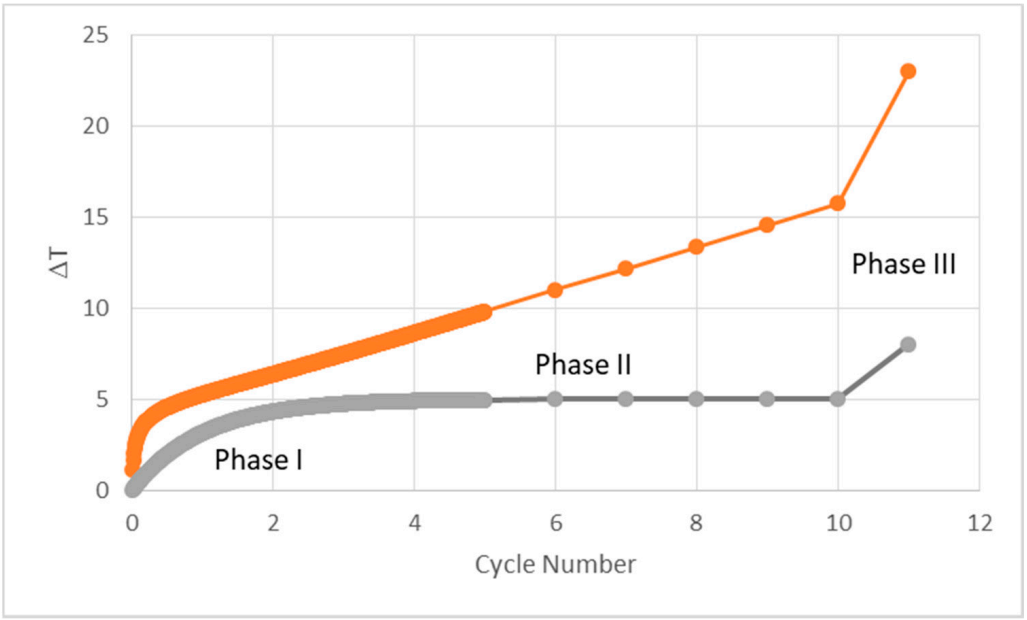

Figure 2. Typical temperature evolution curve during fatigue test.

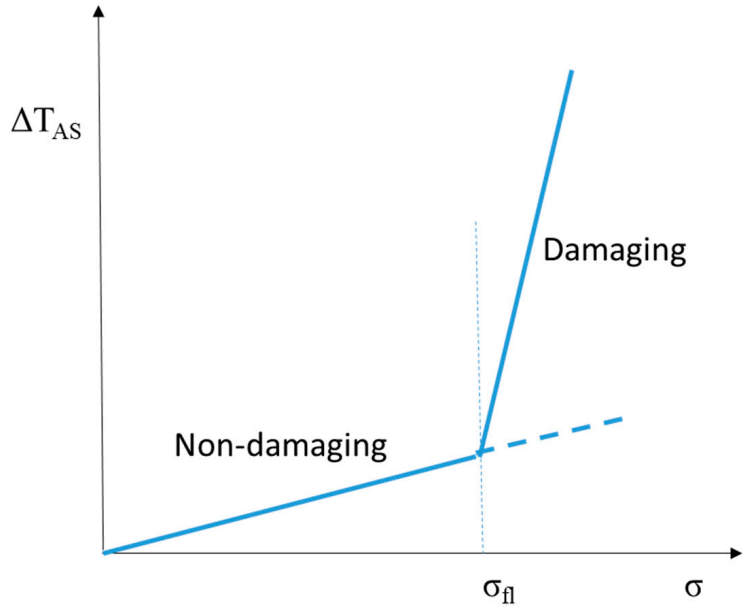

Figure 3. A schematic ΔT_{AS} vs. σ curve to determine the fatigue endurance limit.

The questions regarding the observed phenomena are:

1. What controls the temperature variation in each phase of self-heating?
2. What is the functional dependence of self-heating temperature ΔT_{AS} on the applied stress amplitude (bilinear as implied by the Risitano method [2], or curved as observed by Guo et al. [22])?
3. What is the relationship between the dissipation energy (or ΔT_{AS}) and fatigue damage (life)?

The answers to Q1 are often sought from the laws of thermodynamics, as will be discussed later in Sections 3, 3.1 and 3.2. The answers to Q2 and Q3 are still phenomenologically-based. Once the stress-dependence functions of self-heating are derived from the underlying physical mechanisms, the fatigue endurance limit can be deduced from the "damaging" self-heating mechanism(s).

3. The Thermodynamic Framework

The thermodynamic framework for heat generation and energy dissipation at the macroscopic level is given by the continuum thermodynamics [44]. For a deformable body, the first principle of thermodynamics states that:

$$\dot{E} = \dot{W} + \dot{Q} = \frac{d}{dt}\int_{\mathfrak{D}} \rho e \, dV = \int_{\mathfrak{D}} \sigma : \dot{\varepsilon} dV + \int_{\mathfrak{D}} r \, dV - \int_{\partial\mathfrak{D}} q \cdot n \, dS \tag{1}$$

where ρ is the mass density, e is the specific internal energy, σ is the Cauchy stress tensor, $\dot{\varepsilon}$ is the total strain rate tensor, the symbol ":" signifies the scalar product of tensors, r is an external heat source, q is the heat flow vector through the material surface (with the normal vector n) of the material volume $\mathfrak{D}$.

By the divergence theorem (Gauss's theorem), Equation (1) turns into

$$\rho \dot{e} = \sigma : \dot{\varepsilon} + r - \nabla \cdot q \tag{2}$$

The second law of thermodynamics requires that the local heat generation satisfies the Clausius–Duhem inequality:

$$\rho \dot{s} - \frac{r}{T} + \nabla \cdot \left(\frac{q}{T}\right) \geq 0 \tag{3}$$

where s is the specific entropy, T is the absolute temperature.

Introducing the Helmholtz free energy, as:

$$\psi = e - Ts \tag{4}$$

Combining Equations (2)–(4) leads to:

$$\sigma : \dot{\varepsilon} - \rho\dot{\psi} - s\dot{T} - q \cdot \frac{\nabla T}{T} \geq 0 \tag{5}$$

The thermodynamic equilibrium of a homogenous control volume can be identified with local state variables: $\varepsilon = \varepsilon_e + \varepsilon_p$, T, α, which represents respectively, the total strain (the sum of elastic and plastic strains), the absolute temperature, and internal state variables of the material element. The free energy and the entropy are state functions of these variables, i.e., $\psi = \psi(\varepsilon_e, T, \alpha)$ and $s = -\partial\psi/\partial T$ (according to the second law of thermodynamics requirements) [44]. Then, the rate of change of these state functions are:

$$\dot{\psi} = \frac{\partial \psi}{\partial \varepsilon_e}\dot{\varepsilon}_e + \frac{\partial \psi}{\partial T}\dot{T} + \frac{\partial \psi}{\partial \alpha}\dot{\alpha} \tag{6}$$

$$\dot{s} = \frac{\partial s}{\partial \varepsilon_e}\dot{\varepsilon}_e + \frac{\partial s}{\partial T}\dot{T} + \frac{\partial s}{\partial \alpha}\dot{\alpha} = -\frac{\partial^2 \psi}{\partial \varepsilon_e \partial T}\dot{\varepsilon}_e - \frac{\partial^2 \psi}{\partial T^2}\dot{T} - \frac{\partial^2 \psi}{\partial \alpha \partial T}\dot{\alpha} \tag{7}$$

$$\dot{e} = \dot{\psi} + T\dot{s} + s\dot{T} \tag{8}$$

With the specific heat defined as $c_p = -T \cdot \partial^2\psi/\partial T^2$ and $q = -k\nabla T$ (k is thermal conductivity), the first law of thermodynamics can be written as [44]:

$$\rho c_p \dot{T} - k\nabla^2 T = \sigma : \dot{\varepsilon}_p + \rho T \frac{\partial^2 \psi}{\partial \varepsilon \partial T} : \dot{\varepsilon}_e - \rho\left(\frac{\partial \psi}{\partial \alpha} - T\frac{\partial^2 \psi}{\partial \alpha \partial T}\right)\dot{\alpha} + r \tag{9}$$

This is the heat equation governing heat generation, dissipation, and transfer processes. Note that basically the same formulation has been adopted in the previous self-heating-thermographic studies [7,8,16,22,42,43]. For coupons under uniform stress conditions, $\nabla T = 0$.

Generally, the heat sources (the terms on the right side of Equation (9)) can be classified as d_1, s_{the}, s_{ic}, and r, which stands for the intrinsic (mechanical) dissipation source, thermo-elastic source, "internal" coupling source and external heat supply, respectively, as follows [7,43]:

$$d_1 = \sigma : \dot{\varepsilon}_p - \rho\frac{\partial \psi}{\partial \alpha}\dot{\alpha} \tag{10}$$

$$s_{the} = \rho T \frac{\partial^2 \psi}{\partial \varepsilon \partial T} : \dot{\varepsilon}_e \tag{11}$$

$$s_{ic} = \rho T \frac{\partial^2 \psi}{\partial \alpha \partial T}\dot{\alpha} \tag{12}$$

When a coupon test is designed with a gauge section being uniformly stressed, if we only consider intrinsic mechanical dissipation as the only heat source for argument sake, Equation (9) turns into the following form [8,19]:

$$\rho c_p\left(\dot{\theta} + \frac{\theta}{\tau_{eq}}\right) = d_1 \tag{13}$$

where $\theta = T - T_0$ (T_0 is initial temperature), $\tau_{eq} = \frac{\rho c_p V}{Ah}$, h is the heat transfer coefficient, A is the surface area, and V is the volume of the specimen gauge section.

The solution of Equation (13) is [8]:

$$\theta = \frac{\tau_{eq} d_1}{\rho c_p}\left(1 - e^{-\frac{t}{\tau_{eq}}}\right) \tag{14}$$

Upon initial loading, the coupon surface temperature is close to the ambient environment, the heat generation rate is constant, $\dot{\theta} = d_1/\rho c_p$. In Phase I, the incremental temperature rate gradually decreases as heat dissipation, by means of heat convection through the specimen surfaces, increases. When it comes to phase II, self-heating temperature stabilization occurs, and it remains constant for a prolonged period. This stabilization is reached due to the equilibrium between the thermal energy generated from self-heating, and the thermal energy outgoing to the environment through convection and radiation (often negligible). Equation (14) describes the phase I–II behavior. A self-heating scenario depends on the level of applied stress. In some cases, e.g., [9,23,25], the thermal equilibrium does not occur, and the second phase is characterized by a temperature increase at a nearly constant rate. This phenomenon can be induced by several mechanisms, such as cyclic microstructural changes and progressive damage development in the form of voids and microcracks. These topics need to be further characterized with the aid of metallographic examinations, which are beyond the scope of the present paper. When microcracks accumulate, it ends phase II of self-heating and triggers phase III. Phase III is characterized by an accelerating temperature increase, as the process is dominated by the frictional heating at a macroscopic scale, i.e., the newly appeared surfaces of a propagating crack start to slide against each other under cyclic loading, leading to changes in calorimetric performance.

To describe the self-heating phenomena (without external heat sources, $r = 0$), it is important to understand the internal heat sources associated with different deformation and dissipation mechanisms, which will be discussed in the following.

3.1. Elastic Deformation

When deformation is purely elastic, i.e., $\varepsilon = \varepsilon_e$, $\sigma = \partial\psi/\partial\varepsilon_e$ [44], and there is no change of material internal state ($\dot{\alpha} = 0$), then the only heat generation term left on the right side of Equation (9) is [8]:

$$s_{the} = \rho T \frac{\partial^2 \psi}{\partial \varepsilon \partial T} : \dot{\varepsilon} = \rho T \frac{\partial \sigma}{\partial T} : \dot{\varepsilon} \tag{15}$$

This means the heat generation occurs by thermoelasticity only, where $\frac{\partial \sigma}{\partial T} = \alpha_T E$, α_T is the coefficient of thermal expansion, E is Young's modulus of the material. Thus, the thermoelasticity-generated heat depends linearly on the applied strain rate $\dot{\varepsilon}$ which is linearly proportional to the stress amplitude σ_a and frequency f in elastic deformation. In flat coupon fatigue testing, this term is usually small along the order of <1 °C under cyclic loading at the ambient background temperature [8], which has minimal effect on fatigue.

3.2. Internal Friction

Internal friction generally refers to the motion of rubbing between microstructural elements in the material. This may lead not only to heat generation but also to damping and fatigue, causing, depending on the stress amplitude, reversible or irreversible deformation. In metals under cyclic loading at low amplitudes, dislocation segments may bow back and forth between weak pinning points [20–22,30]. Even though at the macroscopic level the deformation process is reversible, restricted dislocation glide does occur. Once the stress amplitude exceeds the overall lattice resistance, dislocations can break away from pinning and glide freely along crystallographic planes throughout the lattice, resulting in micro- or macro-plastic deformation. Therefore, before irreversible dislocation motion occurs, there should be no change in the material microstructure and internal energy, so the right side of Equation (9) reduces to (neglecting the thermoelastic and internal state variable-related terms):

$$d_1 = \sigma : \dot{\varepsilon}_p \tag{16}$$

where d_1 represents the hysteresis energy due to anelastic dislocation motion.

Guo et al. studied the thermographic behavior of FV520B stainless steel under different stress amplitudes [22], and they observed that the relationship of dissipation energy vs. stress amplitude (d_1 vs. σ) exhibits a curve, as shown in Figure 4. They divided the curve

into three stages: (i) pure elastic (reversible), (ii) anelastic internal friction, and (iii) intrinsic dissipation, marked by two critical stresses, σ_{c1} = 179 MPa and σ_{c2} = 400 MPa for the material. The first critical stress corresponded to the deviation from the initial elastic line, i.e., the proportional limit on the tensile curve, below which there was no energy dissipation by pure elasticity. The second critical stress divided the stages of linear and nonlinear dissipation, which was found to be close to the fatigue endurance limit obtained from the conventional fatigue testing [22]. Here, the "bilinear" relationship of the Risitano method is apparently not sufficient to clearly define the "intersection". Between σ_{c1} and σ_{c2}, the dissipation energy appears to be a linear function of the applied stress amplitude. Guo et al. argued that internal friction occurs in the stress range ($\sigma_{c1} < \sigma < \sigma_{c2}$) as a result of the movement of dislocations, but the process returns the atoms to their equilibrium positions, thereby increasing the kinetic energy and temperature because of releasing the excess energy gained during the movement. In this sense, internal friction does not contribute to fatigue damage.

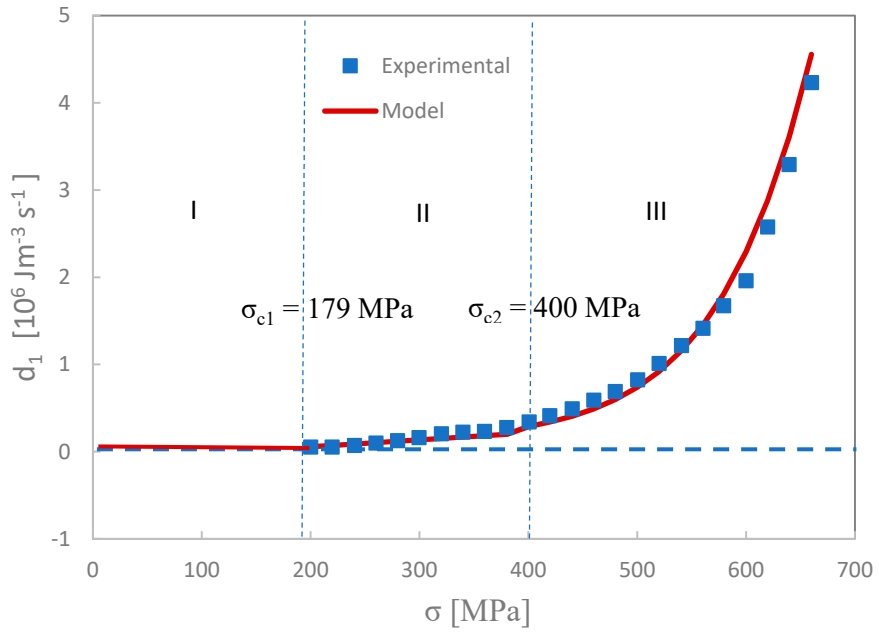

Figure 4. Stress amplitude dependence of the intrinsic dissipation of the FV520B stainless steel. Data are after [22].

3.3. Intrinsic Dissipation

As deformation proceeds into the plastic regime, irreversible deformation occurs with microstructural changes in terms of dislocation structures. From the continuum point of view, attempts to track the development of irreversible processes in the energy balance (the first law of thermodynamics) are to find internal state variables admissible by the second law of thermodynamics, i.e., also satisfying the Clausius-Duhem inequality [22,42–44]. However, due to the limitation of the continuum mechanics that assumes material homogeneity, it seems difficult to uniquely specify the irreversible changes in the microstructure concerning macroscopic strain in the framework of continuum thermodynamics. Nevertheless, a set of internal state variables α_i (i = 1, 2, . . .) are often introduced to represent the effect of irreversible microstructural changes at the continuum level. As far as dissipation at the macroscopic scale is concerned (with a measurable temperature variation), the heat source of internal energy dissipation is given by:

$$d_1 = \sigma : \dot{\varepsilon}_p - \rho \frac{\partial \psi}{\partial \alpha} \dot{\alpha} \tag{17}$$

The first term in Equation (17) represents the hysteresis energy in the cyclic process. The second represents the contributions from irreversible microstructural changes associated with inelastic deformation, i.e., changes in internal state variables, $\dot{\alpha}$. With the involvement of internal state variables, it is even more difficult and often ambiguous to calculate the heat source, d_1, straightly from its definition, using Equation (17). Most often, d_1 is back-calculated from the thermographic measurements.

Guo et al. used a power-law function to describe intrinsic dissipation energy above the critical stress σ_{c2}, as [22]:

$$d_1 = k_d \sigma^p H(\sigma - \sigma_{c2}) \tag{18}$$

where k_d is the proportional constant and p (= 8.05 for FV520B) is the power exponent, $H(x)$ is the Heaviside step function, which equals zero when $x \leq 0$ and equals 1 when $x > 0$.

They further demonstrated that the high cycle fatigue (HCF) life can be expressed by [22]:

$$N_f = \frac{E_C f}{k_d \sigma^p} H^{-1}(\sigma - \sigma_{c2}) \tag{19}$$

where E_C is the energy dissipation threshold for fatigue failure to be determined by fitting with experimental data. The inverse of the Heaviside function implies that fatigue life is infinite at σ_{c2}, which is thus deemed to be fatigue endurance limit.

Intrinsic dissipation occurs by irreversible dislocation motion, which is a damaging process resulting in fatigue under cyclic loading. Heat generation has also been observed in associated with localized slip zones (Lüders band propagation) [47] and martensite transformation [48]. Even though both the internal friction and intrinsic dissipation processes are classified based on dislocation motion mechanisms, the exact stress-dependence functions for each stage are not derived from the underlying physical mechanisms yet, and the division between the damaging/non-damaging stages and the subsequent fatigue damage function (the S-N relation) is still largely phenomenological.

3.4. Damping

Crupi [9] developed a unified approach using thermographic measurements to characterize both damping and HCF. Damping is due to anelastic dislocation motion that creates a lag in phase between the oscillating stress and strain [49,50]. The specific damping capacity is defined as [9]:

$$\psi = \frac{\Delta W}{U} = 4\pi\zeta, \; U = \frac{\Delta\sigma^2}{2E} \tag{20}$$

where ΔW is the hysteresis energy, U is the elastic energy during the cycle, E is Young's modulus, and ζ is the damping ratio. The specific damping capacity can also be measured independently using vibration methods [51]. Thus, Equation (20) provides an independent means to assess the hysteresis energy ΔW and vice versa, for damping. Furthermore, the measure of damping can also be used for non-destructive damage detection [52,53].

The stabilized temperature increment is related to the hysteresis energy by [9]:

$$\Delta T_{AS} = \frac{N_{AS} \Delta W}{\rho c_p} \tag{21}$$

where N_{AS} is the cycle to the stabilized temperature (the cycle number of Phase I)

To correlate with the fatigue life, Crupi further proposed the following relationship [9]:

$$\Delta W_{ToT} = \Delta W \cdot N_f \tag{22}$$

where ΔW_{TOT} is the total energy of fracture, N_f is the number of cycles to fatigue fracture. Here, ΔW_{TOT} is assumed to be constant for the fatigue process.

Crupi observed that ΔT_{AS} was nearly zero when the applied stress is below a certain value, σ_0; and above it,

$$\Delta T_{AS} = \frac{N_{AS}\psi}{2\rho c_p}\left(\Delta\sigma^2 - \sigma_0^2\right) \tag{23}$$

This relationship was experimentally verified on AISI304 steel and AA6082 aluminum alloy welded joints, and σ_0 was found to correspond to the fatigue endurance limit. But, to match the experimental data, i.e., the S-N curve (the Basquin equation), $\Delta\sigma^m N_f = C$, Crupi assumed that $\Delta T_{AS} = A\Delta\sigma^m$, and found m = 6.3 for AA6082 by fitting the S-N curve from the conventional fatigue testing [9]. Apparently, an inconsistency exists between the stress dependence of ΔT_{AS} in Equation (23) as observed by IR thermography and the S-N.

3.5. Fatigue Fracture Entropy

Naderi, Amiri, and Khonsari proposed a fatigue fracture entropy (FEE) concept, which can serve as a measure of fatigue damage [16]. FEE is the cumulative entropy of material up to the fracture. They showed that FEE was nearly constant for the tested materials (Al 6060-T6 and stainless steel 304), independent of specimen geometry, load (bending, tension-compression, torsion, etc.), and frequency.

Mehdizadeh and Khonsari further elaborated the concept for low cycle fatigue (LCF) and high cycle fatigue (HCF) based on the infrared thermographic measurements under the cyclic loadings. They defined the entropy production rate as given by [16,19]:

$$\dot{S} = \frac{Q_t}{T} \tag{24}$$

where $Q_t = \sigma : \dot{\varepsilon}_p$, which can be evaluated from the initial slope, R_θ, of the thermographic curve as:

$$Q_t = \rho c_p R_\theta = \rho c_p \dot{\theta}\Big|_{t=0} \tag{25}$$

Then, the total entropy for the fatigue process is obtained by integration of Equation (24) up to the time of failure, t_f, as:

$$FEE = \int_0^{t_f} \frac{Q_t}{T} dt \approx \frac{N_f}{f T_s} \oint \sigma d\varepsilon_p \tag{26}$$

where T_s is the stabilized temperature, as the major part of self-heating is spent in Phase II, as shown in Figure 2. In the fatigue process, the plastic strain energy per cycle, $\oint \sigma d\varepsilon_p$ (the area of the hysteresis loop), is almost constant [54,55].

Mehdizadeh and Khonsari also applied the FEE concept to the HCF of SS304 and CS1018 steels [19]. As discussed previously, uniform heat generation and dissipation could come from two sources: (i) internal friction involving reversible movement of atoms and dislocations; and (ii) microplastic deformation and formation of microcracks. In LCF, the energy dissipation generated by internal friction could be negligible compared to the plastic hysteresis energy. However, in HCF, the energy dissipation generated by internal friction occurs at a level comparable to microplastic deformation, especially near the fatigue endurance limit. Therefore, for HCF, the initial temperature increase rate R_θ could consist of two parts: (i) the part related to internal friction (R_θ^f)—which is non-damaging—and (ii) the part related to microplastic deformation and microcrack nucleation (R_θ^p), which is damaging. Accordingly,

$$Q_t = Q_t^p + Q_t^f = \rho c_p R_\theta^p + \rho c_p R_\theta^f \tag{27}$$

The fatigue fracture entropy in HCF can be defined concerning the plastic energy generation (Q_t^p) as:

$$FEE = \frac{N_f Q_t^p}{f T_s} \tag{28}$$

Similar to the behavior observed by Guo et al. (Figure 4), Mehdizadeh and Khonsari observed for SS 304 and CS 1018 that linear dependence of R_θ on stress below the fatigue endurance limit, and there was a sudden increase in the curve of R_θ versus the stress amplitude above that. They attributed the low slope R_θ^f to internal friction. As the stress increases, the portion of R_θ^f in the total R_θ ($= R_\theta^p + R_\theta^f$) becomes insignificant as compared to R_θ^p, which means intrinsic dissipation would dominate the self-heating process above the fatigue endurance limit. They used the Morrow energy approach to characterize the relationship between the stress amplitude and the fatigue life [20,22].

3.6. The Tanaka-Mura-Wu Model

It has been well understood from the physical metallurgy point of view that metal fatigue is a process involving alternating slips under cyclic loading, leading to the formation of persistent slip bands, and eventually crack nucleation and propagation. Crystallographic slip is the mechanism of plastic deformation at both macro and microscopic scales. A tremendous amount of literature exists on this topic, but due to the limited space, it cannot all be cited in this article, except that readers are referred to see Deformation and Life Evolution in Crystalline Materials [46].

Tanaka and Mura [56] developed a theoretical model where fatigue crack nucleation is envisaged to occur via the accumulation of dislocation dipole pile-ups within the slip band. At the surface, these dislocation dipole pile-ups appear to be intrusion/extrusions, as shown in Figure 5. Dislocation pile-ups can also nucleate intergranular microcracks at their intersections with grain boundaries [57]. Scenarios of the heterogeneity of persistent slip band evolution are still of interest in current metallurgical studies [58]. Despite that, the Tanaka-Mura model does not cover all the complicated scenarios in real materials, but serves as a physical baseline from which mathematical derivations could proceed, as given in the following.

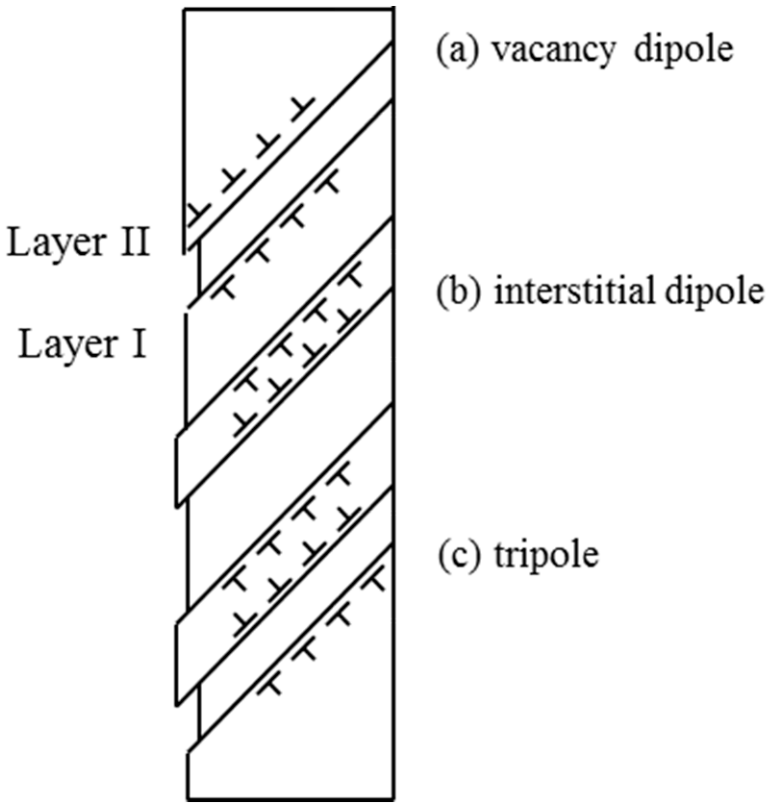

Figure 5. Dislocations in (**a**) vacancy dipoles (forming an intrusion), (**b**) interstitial dipoles (forming an extrusion) and (**c**) tripoles (forming an intrusion-extrusion pair) at the surface.

In the original Tanaka-Mura model, the plastic strain of dislocation pile-up was calculated by displacement integration, which resulted in a physical dimension of m^2 in the strain unit. Recently, Wu [45] revisited the Tanaka-Mura model and revised the plastic strain expression using the true strain definition. In the revised model, hereafter called the Tanaka-Mura-Wu (TMW) model, the dislocation pile-up energy is given by [45,56]:

$$\Delta U_c = \frac{1}{2}(\Delta\tau - 2k)\Delta\gamma \tag{29}$$

where $\Delta\tau$ is the applied shear stress range, k is the lattice friction resistance, and $\Delta\gamma$ is the plastic strain range given by [45]:

$$\Delta\gamma = \frac{2(1-v)(\Delta\tau - 2k)}{\mu} \tag{30}$$

where μ is the shear modulus and v is Poisson's ratio.

When the total accumulated energy is equal to the energy of forming new crack surfaces of 2a by the Griffith criterion [45,56]:

$$N\Delta U_c ba = 2w_s a \tag{31}$$

where a is the crack nucleation size (dislocation pile-up length), b the Burgers vector, and w_s the surface energy, J/m^2.

Equation (31) can be turned into [45]

$$N_f = \frac{8(1-v)w_s R_s}{\mu b}\frac{1}{\Delta\gamma^2} \tag{32}$$

or

$$N_f = \frac{2\mu w_s}{(1-v)b}\frac{1}{(\Delta\tau - 2k)^2} \tag{33}$$

It is noted that a surface roughness factor R_s (=1 for ideally smooth surface, e.g., electropolished; ≈1/3 for machined surface) is introduced into the strain-life equation, Equation (32), as it could affect the local intrusion/extrusions, while in the stress-life equation its effect is hidden in k to reduce the coupon fatigue limit. Under uniaxial loading conditions, the shear stress/strain ranges can be converted to the normal stress/strain by the Taylor factor: $\Delta\tau = \Delta\sigma/\sqrt{3}$, $\Delta\gamma = \sqrt{3}\Delta\varepsilon$.

Equations (32) and (33) express the fatigue crack nucleation life explicitly in terms of the elastic modulus, the Burgers vector, and the surface energy of the material, which has been validated against LCF experiments on copper, titanium, tungsten, Type 316 stainless steel, Waspaloy, and MAR-M 509 [45], and recently extended to the full range fatigue life of many engineering alloys of Al, Ti, Fe, and Ni-base families, equiatomic high entropy alloy (HEA) CoCrFeMnNi [59], as well as additive manufactured materials [60].

Here, the first case study is to compare the TMW model, Equation (33), with the S-N data (σ_0 = 101 MPa) from Crupi's study [9], as shown in Figure 6. The aluminum alloy properties used in the calculation are: μ = 27 GPa, v = 0.3, w_s = 1.125 J/m^2, $b = 2.86 \times 10^{-10}$ m (same as 7075-T6 and 2024-T3 in [59]), and $2k = 101/\sqrt{3}$ MPa. It can be seen that the agreement between the experimental and predicted life is very well.

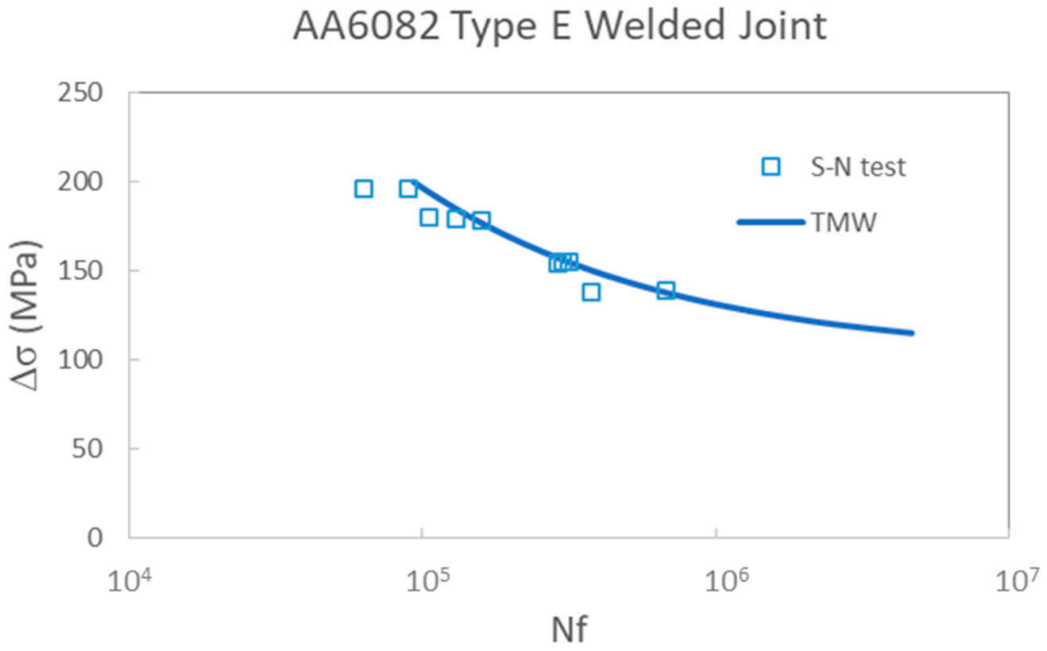

Figure 6. S–N data from fatigue tests including thermographic fatigue tests (data after [9]) and the curve by the TMW model for aluminum alloy AA6082 type E welded joint.

The second case study takes the experimental data from Meneghetti and Ricotta [12]. Uniaxial strain-controlled fully reversed (R = −1) fatigue tests were conducted on SS304L at frequencies between 0.1 and 5 Hz. The test frequency was selected to limit the stabilized temperature below 70 °C. In the medium and high cycle fatigue regimes, tests were run at the highest frequency compatible with the available experimental equipment. The cyclic stress-strain curve (connecting peak points of the stabilized hysteresis loops) was described by the Ramberg-Osgood equation:

$$\varepsilon = \varepsilon_e + \varepsilon_p = \frac{\sigma}{E} + \left(\frac{\sigma}{K'}\right)^{\frac{1}{n'}} \tag{34}$$

with K' = 2250 MPa, n' = 0.337 [12].

The experimental fatigue life was given by the Coffin-Manson equation:

$$\varepsilon = \varepsilon_e + \varepsilon_p = \frac{\sigma'}{E}\left(2N_f\right)^b + \varepsilon'_f\left(2N_f\right)^c \tag{35}$$

with σ' = 3641 MPa, b = −0.238, ε'_f = −0.085, c = −0.375 [12].

Using Equation (34) to calculate the plastic strain at the given stress level, and using Equation (32) with E = 193 GPa, w_s = 2.4 J/m^2, b = 2.48 × 10^{-10} m (same as steels in [45,59]), R_s = 1/3 [45] to calculate the fatigue life, the TMW model is compared with the Coffin-Manson relation, as shown in Figure 7. It is seen that the agreement of the TMW model with the experiment is very good. It should be emphasized that, in this calculation, Equation (32) provides class-A predictions without the need for the event data for calibration.

Furthermore, using the stress-life Equation (33), the fatigue endurance limits can be evaluated as follows:

$$\sigma_0 = \sqrt{3}k = \sigma_a - \frac{1}{2}\sqrt{\frac{6\mu w_s}{(1-\nu)bN_f}} \tag{36}$$

where N_f is the endurance cycle limit ~10^7, and σ_a can either be calculated using the Ramberg-Osgood equations or taken from the fatigue test data.

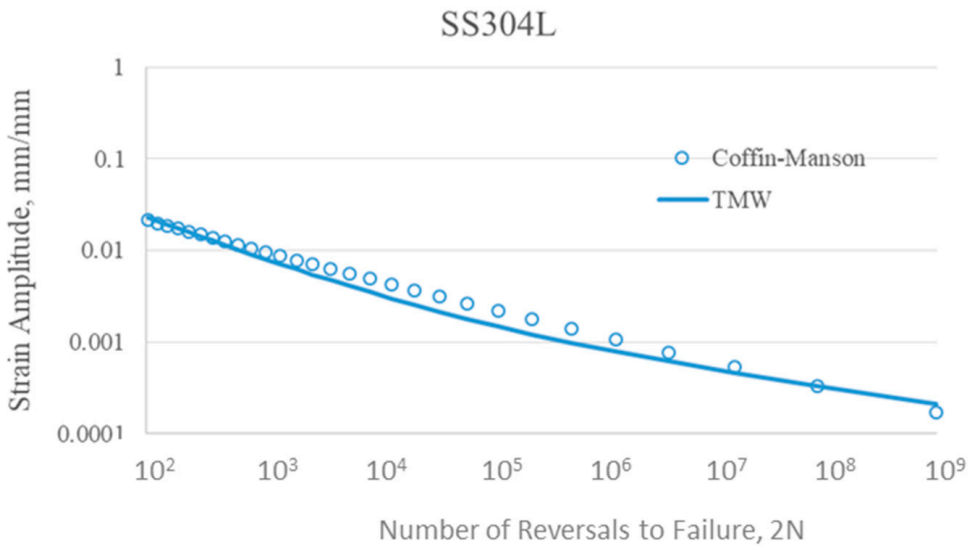

Figure 7. The predicted fatigue life by the TMW model in comparison with the best-fit Coffin-Manson relation for the test data.

Meneghetti and Ricotta, using the calorimetric data from their experiment, assumed that $Q^c 2N_f = const.$ [12], where Q is the heat loss and c is the power exponent, apparently an empirical relation. Both Figures 6 and 7 demonstrate that the TMW model can predict fatigue life, independent of conventional and thermographic fatigue data, which offers huge savings in both time and cost for fatigue design.

3.7. The Energy Argument

As Equation (31) represents the Griffith energy criterion, the dislocation pile-up energy (which later will be converted to crack formation energy) contributed by each cycle in terms of plastic strain is given by combining Equations (29) and (30), as:

$$\Delta U_c = \frac{3\mu}{4(1-v)}(\Delta\varepsilon_p)^2 \tag{37}$$

The crack nucleation energy is calculated to be about 0.2 MJ/(m^3 cycle) at the strain amplitude of 0.16%, which is close to the heat energy Q of 0.3 MJ/(m^3 cycle) measured by Meneghetti and Ricotta [12]. This means a fraction of the mechanical energy would be converted to crack nucleation by forming new crack surfaces. To explain the energy partition, a schematic of the simplified microstructure containing dislocation structures with plastic deformation is shown in Figure 8 (For understanding the dislocation structure in real materials, the readers are referred to look at transmission electron micrographs reported in the literature). A dislocation structure typically consists of slip lines and persistent slip bands, within which dislocation dipole pile-ups also exist (note that only vacancy dipoles are drawn here for the sake of fatigue crack nucleation). At low strain amplitudes, dislocation movement may lead to the formation of a ladder structure with dislocation walls and channels. At high strain amplitudes, it may evolve into labyrinth or cell structures. While the moving dislocations contribute to heat generation by lattice friction, dislocations in the (non-moving) walls cause structural changes, increasing the internal energy and the entropy by increasing the disorder of the lattice. When the dislocation dipole pile-up burst into a crack, the energy stored in the pile-up array converts to the energy of new surface formation, while the energy of those structural dislocations is stored in the material. Thus, the total irreversible work per cycle can be transformed into three parts:

$$\Delta W = \int_{\mathfrak{D}} \int \sigma \, d\varepsilon_p \, dV = \int_{\mathfrak{D}} \Delta U_s \, dV + \int_{\mathfrak{D}} \Delta U_c \, dV + \int_{\mathfrak{D}} \Delta U_h \, dV \tag{38}$$

where U_s is the energy stored in the material with irreversible structural changes, U_c is the work contributing to the energy of fatigue crack nucleation (forming new surfaces), and U_h is the part convertible to heat generation.

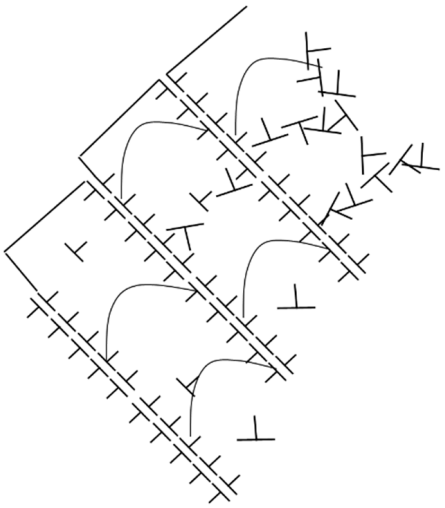

Figure 8. A schematic of microstructure containing a dislocation structure with plastic deformation.

It should be noted that a material coupon in a mechanical testing environment is not an isolated system. The heat generated by self-heating mechanisms in the material coupon will eventually dissipate into the environment, as outgoing heat flux. From Equation (38), it can be inferred that the energy stored for disorder (irreversible structural change), U_s, should always be less than the total mechanical work input. As a material's entropy is almost impossible to be directly calculated by counting the order/disorder of the microstructural change involving dislocation arrangements for a real crystalline material, as expressed by Boltzmann's equation: $S = k_B \ln \Omega$, (k_B is the Boltzmann constant, Ω is the number of microstates that the system will exist relative to all the possible microstates), Equation (38) serves as an indirect means to estimate that, once self-heating is precisely described.

Considering the formation of microcracks as part of the energy process, then the first law of thermodynamics of the deformation process should be:

$$\Delta\Pi = \Delta W_0 + \sum_i \frac{\partial \Delta W}{\partial a_i} \Delta a_i - \Delta Q_h = \Delta W_0 - \sum_i G_i \Delta a_i - \Delta Q_h \tag{39}$$

with

$$G = -\frac{\partial \Delta W}{\partial a} \tag{40}$$

where $\Delta\Pi$ is the total energy, ΔW_0 is the stored strain energy without cracking, a_i is the newly formed crack area, G_i is the Griffith energy release rate [61], and, here, Q_h signifies the heat loss due to energy dissipation.

Three instances can be inferred from Equation (39):

i. In a deformation process without structural changes and cracking, $\Delta\Pi = 0$ and $G = 0$, the dissipated energy (heat) can be equal to the mechanical work input, $\Delta Q_h = \Delta W_0$.

ii. In a deformation process without structural changes, but cracking occurs due to fatigue, e.g., at low strain levels, $\Delta\Pi = 0$ and $G \neq 0$, the dissipated energy (heat) would be equal to the mechanical work less the crack-forming energy, $\Delta Q_h = \Delta W_0 - \sum_i G_i \Delta a_i$.

ii. In a deformation process with significant structural changes and cracking, e.g., at high strain levels, $\Delta\Pi \neq 0$ and $G \neq 0$, the dissipated energy (heat) would be equal to the mechanical work less the structural change and crack-forming energies, $\Delta Q_h = \Delta W_0 - \Delta W_s - \sum_i G_i \Delta a_i = \Delta W_h$, i.e., $\Delta Q_h < \Delta W$.

Instances I and II can be utilized to interrogate fatigue endurance limits using thermographic methods. One of the difficulties in dealing with instance III is that it is hard to formulate the entropy change in a deformed body in terms of internal state variables at the continuum level. An internal state variable can be defined as the cross-sectional area damage parameter ω (=0–1), as in the continuum damage mechanics [44]. As a result, the effective stress is increased as given by $\sigma_{eff} = \sigma/(1 - \omega)$, leading to increased strain energy stored within the material. This would partly account for the increased energy dissipation, or increased temperature, towards the end of the fatigue process. However, additional heat sources may be created along the process: once cracks have been nucleated, mechanical rubbing between the mating crack surfaces will also generate heat during fatigue. Therefore, physical links between the self-heating characteristics and the internal state variables still need to be established, which can be a significant area of future research.

Another subject that needs to be considered along with thermodynamics is ultra-high cycle fatigue (UHCF) with failure cycles exceeding 10^7. The UHCF behavior typically has a duplex S-N curve behavior, where the location of fatigue crack nucleation has been found almost exclusively in the specimen's interior, usually at non-metallic inclusions [62–64]. In this case, local stiffness mismatch between the inclusion and the matrix could induce local stress concentration, as treated by Eshelby [65], and thus cause crack nucleation and subsequent propagation. This article does not mean to give a comprehensive review of the UHCF studies but highlights the important aspects of self-heating.

In UHCF testing (exceeding 10^7 cycles), to achieve the fatigue life results in a matter of days, the loading frequency would have to be in the kHz range [66]. It is then expected that the test results are frequency-dependent. For example, fatigue tests run on 316 LN stainless steel showed that the fatigue lives in air at 10 Hz were longer than those at 700 Hz [67]. It was observed that the specimen temperature reached a maximum of 270 °C during the 700 Hz test. Here, at least two factors, internal crack nucleation and self-heating, are compounded to create a complicated problem of local crack nucleation and heat generation, conduction, and dissipation. The self-heating temperature as high as 270 °C could cause not only thermal degradation of mechanical properties but also induce additional deformation mechanisms such as dynamic strain aging in austenitic steels [68,69]. Pulsed loading and forced air-cooling have been applied to avoid specimen heating, to improve the accuracy and reproducibility of ultrasonic fatigue tests. Within the framework of this article, the overall heat equation, Equation (9), still stands for UHCF, except that the employed cooling techniques effectively changed the thermal boundary conditions of the test coupon. A recent review discussed the usability of UHCF data [70].

4. Conclusions

This paper presents an overview of the self-heating phenomena and continuum thermodynamics framework that formulates energy dissipation and heat generation. It is also emphasized that a mechanistic understanding of the self-heating mechanism/heat source should be achieved to quantify the self-heating effect on fatigue behavior and better define the transition from "non-damaging" to "damaging" self-heating. The main conclusions from this review are as follows.

Infrared thermographic techniques have been developed to interrogate the self-heating phenomena during fatigue testing, which generally undergoes three phases: Phase I with steeply increasing temperature to a stabilized or steady-state, i.e., Phase II, followed by an accelerating temperature increase to specimen rupture, Phase III. The initial slope $\partial T/\partial N$ of Phase I, the stabilized temperature increment ΔT_{AS} in Phase II, and the heat loss slope $\partial T/\partial N$ when the test is stopped in the middle of Phase II are heat generation or heat loss characteristics. The fatigue endurance limit is often sought at the point of intersection of the "non-damaging" and "damaging" heat generation curves (e.g., ΔT_{AS} vs. stress relations). As the thermographic method only depends on the data to establish the stabilized Phase II, not to failure), it may provide a rapid alternative means to determine the fatigue endurance limit.

A continuum thermodynamics framework has been established from which the heat equation is derived as the balance between mechanical work input, heat generation and conduction (with convection as the boundary condition), and an increase in the internal energy. Heat sources are expressed as (i) hysteresis energy due to internal friction/intrinsic dissipation, (ii) thermoelastic energy, and (iii) energy arising from changes of internal state variables. The second law of thermodynamics or the Clausius-Duhem inequality permits a set of internal state variables as long as the product with their thermodynamic conjugate forces are greater than zero. However, within the continuum framework, which assumes the material is homogenous, the exact entropy production due to internal structural changes is unknown.

In general, the heat generation processes include (i) thermoelasticity, internal frictions, and (iii) intrinsic dissipation. Internal friction involves dislocation bowing back and forth between weak pinning points, and returning to their original lattice position once the stress is removed, which is a form of anelastic dislocation motion. Intrinsic dissipation occurs by irreversible dislocation motion at either or both macro/microscopic scales, depending on the load level, which will eventually lead to fatigue crack nucleation. For irreversible processes, e.g., fatigue, the increase in internal energy is comprised of energy stored in structural changes (entropy increase) and energy dissipated into heat (self-heating), as well as energy to be released by cracking.

The Tanaka-Mura-Wu model, based on the dislocation dipole pile-up and release of its energy to form new crack surfaces, is shown to provide class-A predictions for fatigue crack nucleation life in terms of the material's elastic modulus, the Burgers vector, the surface energy, and the cyclic stress or plastic strain range. Therefore, it can predict fatigue life, independent of conventional and thermographic fatigue testing.

Regarding the energy argument, according to the first law of thermodynamics, the heat-dissipated energy, Q_h, is contributed partly via the irreversible mechanical work, ΔW. In deformation processes with structural changes and crack formation, $Q_h < \Delta W$. Only until each working term is rigorously derived from the underlying physical mechanisms can the heat energy dissipation be accurately described, and thus defining the fatigue endurance limit through calorimetric analysis could be physically proven and established.

Author Contributions: Conceptualization, L.L. and X.W.; methodology, X.W.; validation, X.W.; formal analysis, X.W.; investigation, L.L.; data curation, X.W.; writing—original draft preparation, X.W.; writing—review and editing, X.W. and L.L.; visualization, X.W.; project administration, X.W. All authors have read and agreed to the published version of the manuscript.

Funding: This research received no external funding.

Institutional Review Board Statement: Not applicable.

Informed Consent Statement: Not applicable.

Data Availability Statement: The data presented in this study are digitized from the published papers (see the corresponding references) and re-analyzed.

Acknowledgments: The authors would like to acknowledge that this study was conducted within the Aeronautical Product Development and Certification Program of the National Research Council Canada.

Conflicts of Interest: The authors declare no conflict of interest.

References

1. Wöhler, A. Wöhler's experiments on the strength of metals. *Engineering* **1867**, *4*, 1373–1380.
2. La Rosa, G.; Risitano, A. Thermographic methodology for rapid determination of the fatigue limit of materials and mechanical components. *Int. J. Fatigue* **2000**, *22*, 65–73. [CrossRef]
3. Luong, M.P. Fatigue limit evaluation of metals using an infrared thermographic technique. *Mech. Mater.* **1998**, *28*, 155–163. [CrossRef]
4. Yang, B.; Liaw, P.K.; Wang, H.; Jiang, L.; Huang, J.Y.; Kuo, R.C. Thermographic investigation of the fatigue behavior of reactor pressure vessel steels. *Mater. Sci. Eng. A* **2001**, *314*, 131–139. [CrossRef]

5. Morabito, A.E.; Dattoma, V.; Galietti, U. Energy-analysis of fatigue damage by thermographic technique. In *XXIV Thermosense Conference*; Maldague, X.P., Rozlosnick, A.E., Eds.; SPIE: Bellingham WA, USA, 2002; Volume 4710, pp. 460–467.
6. Fargione, G.; Geraci, A.; La Rosa, G.; Risitano, A. Rapid determination of the fatigue curve by the thermographic method. *Int. J. Fatigue* **2002**, *24*, 11–19. [CrossRef]
7. Chrysochoos, A.; Louche, H. An infrared image processing to analyse the calorific effects accompanying strain localisation. *Int. J. Eng. Sci.* **2000**, *38*, 1759–1788. [CrossRef]
8. Boulanger, T.; Chrysochoos, A.; Mabru, C.; Galtier, A. Calorimetric analysis of dissipative and thermoelastic effects associated with the fatigue behavior of steels. *Int. J. Fatigue* **2004**, *26*, 221–229. [CrossRef]
9. Crupi, V. An unifying approach to assess the structural strength. *Int. J. Fatigue* **2008**, *30*, 1150–1159. [CrossRef]
10. Liakat, M.; Khonsari, M. Rapid estimation of fatigue entropy and toughness in metals. *Mater. Des.* **2014**, *62*, 149–157. [CrossRef]
11. Meneghetti, G. Analysis of the fatigue strength of a stainless steel based on the energy dissipation. *Int. J. Fatigue* **2007**, *29*, 81–94. [CrossRef]
12. Meneghetti, G.; Ricotta, M. The use of the specific heat loss to analyse the low-and high-cycle fatigue behaviour of plain and notched specimens made of a stainless steel. *Eng. Fract. Mech.* **2012**, *81*, 2–16. [CrossRef]
13. Meneghetti, G.; Ricotta, M.; Atzori, B. A synthesis of the push-pull fatigue behaviour of plain and notched stainless steel specimens by using the specific heat loss. *Fatigue Fract. Eng. Mater. Struct.* **2013**, *36*, 1306–1322. [CrossRef]
14. Amiri, M.; Khonsari, M. Life prediction of metals undergoing fatigue load based on temperature evolution. *Mater. Sci. Eng. A* **2010**, *527*, 1555–1559. [CrossRef]
15. Amiri, M.; Khonsari, M. Rapid determination of fatigue failure based on temperature evolution: Fully reversed bending load. *Int. J. Fatigue* **2010**, *32*, 382–389. [CrossRef]
16. Naderi, M.; Amiri, M.; Khonsari, M. On the thermodynamic entropy of fatigue fracture. *Proc. Roy. Soc. Lond. A* **2010**, *466*, 423–438. [CrossRef]
17. Amiri, M.; Khonsari, M. On the role of entropy generation in processes involving fatigue. *Entropy* **2011**, *14*, 24–31. [CrossRef]
18. Liakat, M.; Khonsari, M. On the anelasticity and fatigue fracture entropy in high-cycle metal fatigue. *Mater. Des.* **2015**, *82*, 18–27. [CrossRef]
19. Mehdizadeh, M.; Khonsari, M. On the role of internal friction in low-and high-cycle fatigue. *Int. J. Fatigue* **2018**, *114*, 159–166. [CrossRef]
20. Guo, Q.; Guo, X. Research on high-cycle fatigue behavior of FV520B stainless steel based on intrinsic dissipation. *Mater. Des.* **2016**, *90*, 248–255. [CrossRef]
21. Guo, Q.; Guo, X.; Fan, J.; Syed, R.; Wu, C. An energy method for rapid evaluation of high-cycle fatigue parameters based on intrinsic dissipation. *Int. J. Fatigue* **2015**, *80*, 136–144. [CrossRef]
22. Guo, Q.; Zaïri, F.; Guo, X. An intrinsic dissipation model for high-cycle fatigue life prediction. *Int. J. Mech. Sci.* **2018**, *140*, 163–171. [CrossRef]
23. Wang, X.G.; Crupi, V.; Jiang, C.; Guglielmino, E. Quantitative Thermographic Methodology for fatigue assessment and stress measurement. *Int. J. Fatigue* **2010**, *32*, 1970–1976. [CrossRef]
24. Wang, X.G.; Crupi, V.; Jiang, C.; Guglielmino, E. Quantitative Thermographic Methodology for fatigue life assessment in a multiscale energy dissipation framework. *Int. J. Fatigue* **2015**, *81*, 249–256. [CrossRef]
25. Zhang, L.; Liu, X.S.; Wu, S.H.; Ma, Z.Q.; Fang, H.Y. Rapid determination of fatigue life based on temperature evolution. *Int. J. Fatigue* **2013**, *54*, 1–6. [CrossRef]
26. Sun, Y.-J.; Hu, L.-S. Assessment of low cycle fatigue life of steam turbine rotor based on a thermodynamic approach. *ASME J. Eng. Gas Turbine Power* **2012**, *134*, 064504. [CrossRef]
27. Imanian, A.; Modarres, M. A thermodynamic entropy approach to reliability assessment with applications to corrosion fatigue. *Entropy* **2015**, *17*, 6995–7020. [CrossRef]
28. Sosnovskiy, L.A.; Sherbakov, S.S. Mechanothermodynamic entropy and analysis of damage state of complex systems. *Entropy* **2016**, *18*, 268. [CrossRef]
29. Wang, J.; Yao, Y. An entropy based low-cycle fatigue life prediction model for solder materials. *Entropy* **2017**, *19*, 503. [CrossRef]
30. Maquin, F.; Pierron, F. Heat dissipation measurements in low stress cyclic loading of metallic materials: From internal friction to micro-plasticity. *Mech. Mater.* **2009**, *41*, 928–942. [CrossRef]
31. Naderi, M.; Khonsari, M. Thermodynamic analysis of fatigue failure in a composite laminate. *Mech. Mater.* **2012**, *46*, 113–122. [CrossRef]
32. Meneghetti, G.; Quaresimin, M. Fatigue strength assessment of a short fiber composite based on the specific heat dissipation. *Compos. Eng. B* **2011**, *42*, 217–225. [CrossRef]
33. Colombo, C.; Vergani, L.; Burman, M. Static and fatigue characterisation of new basalt fibre reinforced composites. *Compos. Struct.* **2012**, *94*, 1165–1174. [CrossRef]
34. Montesano, J.; Fawaz, Z.; Bougherara, H. Use of infrared thermography to investigate the fatigue behavior of a carbon fiber reinforced polymer composite. *Compos. Struct.* **2013**, *97*, 76–83. [CrossRef]
35. Colombo, C.; Libonati, F.; Pezzani, F.; Salerno, A.; Vergani, L. Fatigue behaviour of a GFRP laminate by thermographic measurements. *Procedia Eng.* **2011**, *10*, 3518–3527. [CrossRef]
36. Guagliano, M.; Colombo, C.; Libonati, F.; Vergani, L. Fatigue damage in GFRP. *Int. J. Struct. Integr.* **2012**, *3*, 424–440. [CrossRef]

37. Libonati, F.; Vergani, L. Damage assessment of composite materials by means of thermographic analyses. *Compos. Part B Eng.* **2013**, *50*, 82–90. [CrossRef]
38. Quaresimin, M. *Fatigue of Woven Composite Laminates under Tensile and Compressive Loading*; ECCM-10: Brugge, Belgium, 2002; pp. 3–7.
39. Krasnobrizha, A.; Gorneta, L.; Rozycki, P.; Cosson, P. Rapid determination of the fatigue limit by the simulation of self-heating test by the collaborative model based on the fractional derivative approach. *Procedia Eng.* **2018**, *213*, 192–206. [CrossRef]
40. Elsherbini, Y.M.; Hoa, S.V. Fatigue threshold-stress determination in AFP laminates containing gaps using IR thermography. *Compos. Sci. Technol.* **2017**, *146*, 49–58. [CrossRef]
41. Tong, X.; Chen, X.; Xu, J.-S.; Zheng, Y.; Zhi, S.-J. The heat build-up of a polymer matrix composite under cyclic loading: Experimental assessment and numerical simulation. *Int. J. Fatigue* **2018**, *116*, 323–333. [CrossRef]
42. Shen, F.; Kang, G.; Lam, Y.C.; Liu, Y.; Zhou, K. Thermo-elastic-viscoplastic-damage model for self-heating and mechanical behavior of thermoplastic polymers. *Int. J. Plast.* **2019**, *121*, 227–243. [CrossRef]
43. Huang, J.; Garnier, C.; Pastor, M.-L.; Gong, X. Investigation of self-heating and life prediction in CFRP laminates under cyclic shear loading condition based on the infrared thermographic data. *Eng. Fract. Mech.* **2020**, *229*, 106971. [CrossRef]
44. Lemaitre, J.; Chaboche, J.L. *Mechanics of Solid Materials*; Cambridge Press: Cambridge, UK, 1990.
45. Wu, X.J. *Deformation and Evolution of Life in Crystalline Materials—The Integrated Creep-Fatigue Theory*; CRC Press: Boca Raton, FL, USA, 2019.
46. Wu, X.J. On Tanaka-Mura's fatigue crack nucleation model and validation. *Fatigue Fract. Eng. Mater. Struct.* **2019**, *41*, 894–899. [CrossRef]
47. Louche, H.; Chrysochoos, A. Thermal and dissipative effects accompanying Lüders band propagation. *Mater. Sci. Eng. A* **2001**, *307*, 15–22. [CrossRef]
48. Balandraud, X.; Chrysochoos, A.; Leclercq, S.; Peyroux, R. Influence of the thermomechanical coupling on the propagation of a phase change front. *Comptes Rendus L'academie Des. Sci.—Ser. IIB—Mech.* **2001**, *329*, 621–626.
49. Granato, A.V.; Lücke, K. Theory of mechanical damping due to dislocations. *J. Appl. Phys.* **1956**, *27*, 583–593. [CrossRef]
50. Granato, A.V.; Lücke, K. Application of dislocation theory to internal friction phenomena at high frequencies. *J. Appl. Phys.* **1956**, *27*, 789–805. [CrossRef]
51. Audenino, A.L.; Calderale, P.M. The measure of non-linear internal damping in metals: Processing of decay signal in uniaxial stress field. *J. Sound Vibr.* **1996**, *198*, 395–409. [CrossRef]
52. Kyriazoglou, C.; Le Page, B.H.; Guild, F.J. Vibration damping for crack detection in composite laminates. *Compos. Part A* **2004**, *35*, 945–953. [CrossRef]
53. Kawiecki, G. Modal damping measurement for damage detection. *Smart Mater. Struct.* **2001**, *10*, 466–471. [CrossRef]
54. Morrow, J. Cyclic plastic strain energy and fatigue of metals. *ASTM STP* **1965**, *378*, 45–87.
55. Halford, G. The energy required for fatigue (Plastic strain hysteresis energy required for fatigue in ferrous and nonferrous metals). *J Mater.* **1966**, *1*, 3–18.
56. Tanaka, K.; Mura, T. A dislocation model for fatigue crack initiation. *J. Appl. Mech.* **1981**, *48*, 97–103. [CrossRef]
57. Man, J.; Obrtlík, K.; Polák, J. Extrusions and Intrusions in Fatigued Metals, Part 1 and Part 2. *Phil. Mag.* **2009**, *89*, 1295–1336. [CrossRef]
58. Lavenstein, S.; Gu, Y.; Madisetti, D.; El-Awady, J.A. The heterogeneity of persistent slip band nucleation and evolution in metals at the micrometer scale. *Science* **2020**, *370*, eabb2690. [CrossRef]
59. Li, S.; Liu, R.; Wu, X.J.; Zhang, Z. Full-range fatigue life prediction of metallic materials using Tanaka-Mura-Wu model. *SAE Int. J. Mater. Manuf.* **2022**, *2016*, 15. [CrossRef]
60. Wu, X.; Kanz, P.; Mahmoud, H.; Millar, J.; Shabani, P.; Torres, J.M. Characterization of the Microstructure and Surface Roughness Effects on Fatigue Life Using the Tanaka–Mura–Wu Model. *Appl. Sci.* **2021**, *11*, 9955. [CrossRef]
61. Griffith, A.A. The phenomena of rupture and flow in solids. *Phil. Trans. R. Soc. Lond. A* **1921**, *221*, 163–198.
62. Nishijima, S.; Kanazawa, K. Stepwise S-N Curve and Fish-eye Failure in Gigacycle Fatigue. *Fatigue Fract. Eng. Mater. Struct.* **1999**, *22*, 601–607. [CrossRef]
63. Sakai, T.; Takeda, M.; Shiozawa, K.; Ochi, Y.; Nakajima, M.; Nakamura, T.; Oguma, N. Experimental Evidence of Duplex S-N Characteristics in Wide Life Region for High Strength Steels. *Fatigue* **1999**, *99*, 573–578.
64. Murakami, Y.; Nomoto, T.; Ueda, T. Factors Influencing the Mechanism of Super-long, Fatigue Failure in Steels. *Fatigue Fract. Eng. Mater. Struct.* **1999**, *22*, 581–590. [CrossRef]
65. Eshelby, J.D. The Determination of the elastic field of an ellipsoidal inclusion, and related problems. *Proc. R. Soc. Lond. A* **1957**, *241*, 376–396.
66. Willertz, L. Ultrasonic Fatigue. *Int. Met. Rev.* **1980**, *2*, 66–78.
67. Tian, H.; Liaw, P.; Wang, H.; Fielden, D.; Strizak, J.; Mansur, L.; DiStefano, J. Influence of Mercury Environment on Fatigue Behavior of Spallation Neutron Source (SNS) Target Container Materials. *Mater. Sci. Eng. A* **2001**, *314*, 140–149. [CrossRef]
68. Hong, S.-G.; Lee, S.-B.; Byun, T.-S. Temperature effect on the low-cycle fatigue behavior of Type 316L stainless steel: Cyclic non-stabilization and an invariable fatigue parameter. *Mater. Sci. Eng. A* **2007**, *457*, 139–147. [CrossRef]

69. Wu, X.J.; Quan, G.C.; Sloss, C. *Low Cycle Fatigue of Cast Austenitic Steel, Fatigue and Fracture Test Planning, Test Data and Analysis, ASTM STP 1598*; Wei, Z., Nikbin, K., McKeighan, P.C., Harlow, D.G., Eds.; ASTM International: West Conshohocken, PA, USA, 2017; pp. 35–57.
70. Fitzka, M.; Schönbauer, B.M.; Rhein, R.K.; Sanaei, N.; Zekriardehani, S.; Tekalur, S.A.; Carroll, J.W.; Mayer, H. Usability of Ultrasonic Frequency Testing for Rapid Generation of High and Very High Cycle Fatigue Data. *Materials* **2021**, *14*, 2245. [CrossRef]